# pBn type short-wavelength infrared photodetector with low dark current based on InGaAs/GaAsSb superlattice absorber

Peng Cao[1,2], Qiandong Zhuang[3], Hongling Peng[1,2], Tiancai Wang[4], Chunxu Song[1,5], Jiaqi Wei[1,5] and Wanhua Zheng[1,2,4,5*]

[1] *Laboratory of Solid State Optoelectronics Information technology, Institute of Semiconductors, Chinese Academy of Sciences, Beijing 100083, China*

[2] *State Key Laboratory on Integrated Optoelectronics, Institute of Semiconductors, Chinese Academy of Sciences, Beijing 100083, China*

[3] *Physics Department, Lancaster University, Lancaster LA1 4YB, UK*

[4] *College of Electronic and Communication Engineering, University of Chinese Academy of Sciences, Beijing 100049, China*

[5] *College of Electronic and Communication Engineering, University of Chinese Academy of Sciences, Beijing 100049, China*

E-mail: whzheng@semi.ac.cn

**Abstract:** In this paper, we demonstrate a pBn type short-wavelength infrared (SWIR) photodetector based on InGaAs/GaAsSb superlattice absorber and AlGaAsSb barrier. Both structural and optical properties of InGaAs/GaAsSb superlattice material grown on InP substrate are presented, and optoelectronic performance of pBn SWIR photodetector device are reported. A cutoff wavelength of 2.2 μm is achieved at 300 K. Furthermore, low dark current density of $2.4\times10^{-3}$ A/cm$^2$ and a peak detectivity of $2.0\times10^{9}$ cm·Hz$^{1/2}$/W at 2 μm under saturated operation voltage -1 V are obtained at 300 K. The high performance of the pBn type SWIR photodetector based on InGaAs/GaAsSb absorber provides robust potential for further fabrication of low dark current SWIR photodetector device.

Short-wavelength infrared (SWIR) photodetectors with a spectral response ranging from 1~3 μm have attracted great interests in recent decades since they can be widely exploited in various fields including LiDAR applications, biomedical sensors, earth observation and gas detection [1-5)]. A great many material systems were used as the absorption layer for fabricating SWIR photodetectors. Currently, HgCdTe (MCT) is commercially mature for SWIR photodetector due to the highly tunable spectral response range [6-8)]. However, MCT materials suffer a weak Hg-Te bond and MCT-based devices are undergoing challenges such as unstable crystal quality and low uniformity for large material areas leading to high cost for fabrication [9-11)]. Another promising candidate for the SWIR detection is high In component InGaAs since the cutoff wavelength extends above 2 μm as the In component increases to values above 0.8 [12-15)]. The unfavorable issue for SWIR photodetector based on high In component InGaAs absorber comes to the large lattice mismatch existing between the high In component InGaAs epi-layer and the InP substrate. As a result, large dislocation density brings out large dark current density which deteriorate the performance of the device. Although many attempts are taken to mediate this large lattice mismatch and suppress dark current, for instance, utilizing graded In component InGaAs buffer layer [16-19)] to dilute the dislocation density during the growth process and inserting barrier layer [20,21)] to suppress dark current, the high In component InGaAs SWIR photodetector still suffer high cost and calibration difficulties in growth process.

Recent years, an advanced material system, InGaAs/GaAsSb type II superlattice (T2SL), becomes an option for detection wavelength around 3 μm. Several works were reported on the design and fabrication of InGaAs/GaAsSb based SWIR photodetectors. K.Miura researched the effect of growth temperature and III/V ratio on the high quality InGaAs/GaAsSb superlattice[22)] Justin Easley et al investigated a pin type InGaAs/GaAsSb T2SL for short wavelength infrared detection by simulating the band diagram and absorption spectrum as well as the quantum efficiency diagram[23)]. I.Shafir et al demonstrated pBp type InGaAs/GaAsSb SWIR photodetector, presenting dark current density of $1.3\times10^{-6}$ A/cm$^2$ under 0.1 V operation[24)]. In addition, Tan et al proposed models for SWIR photodetector based on both InGaAs/GaAsSb lattice matched InP and strain compensated InGaAs/GaAsSb, investigating the effect of both total thickness and As component variation of the single period of superlattice on the carrier wavefunction overlap and device cutoff wavelength. This modeling methodology provides further instruction for InGaAs/GaAsSb SWIR photodetector design[25)].

In this paper, we demonstrate a pBn type SWIR photodetector based on InGaAs/GaAsSb absorber and AlGaAsSb barrier. Structural and optical characterization of InGaAs/GaAsSb epi-layer grown on InP substrate is shown and a low dark current down to $2.4\times10^{-3}$ A/cm$^2$ under 300 K is obtained due to the the barrier design. Moreover, a peak detectivity of $2.0\times10^{9}$ cm·Hz$^{1/2}$/W at 2 μm is measured proving this pBn InGaAs/GaAsSb structure to be a promising option for further SWIR photodetector device.

The whole structure of the pBn InGaAs/GaAsSb SWIR device grown on the semi-insulating InP substrate is shown in Figure.1(a). After the deposition of a 500 nm heavily N doped InGaAs bottom contact layer, a 1.75 μm thick lightly N doped InGaAs/GaAsSb absorber is deposited, followed by a 10 nm thick AlGaAsSb barrier layer. Finally, a 200nm thick heavily P doped GaAsSb layer is deposited served as the top contact layer. The device is fabricated by standard photolithography process and the mesa is dry-etched by an inductive coupled plasma (ICP) instrument, followed by a 200 nm thick $SiO_2$ layer deposition over the sidewall by plasma-enhanced chemical vapor deposition (PECVD) for passivation. The X-ray diffraction (XRD) result is shown in Figure.1(b). According to the XRD pattern, the first peak on the left side of the 0$^{th}$ peak stands for both InGaAs epi-layer and InP substrate. The great coincidence indicates the InGaAs layer is lattice match to the InP substrate with an extracted In component of 0.533. The lower peak attached to the 0$^{th}$ peak on the right side represents the GaAsSb material, showing a deviation from the InP substrate. The actual extracted As component of GaAsSb layer is 0.56, which produces a tensile strain of 0.4% during the growth process. Thus, high quality InGaAs/GaAsSb absorber is obtained.

Figure.1(c) characterize the power dependent photoluminescence (PL) spectra of the whole structure. At 300 K, the PL curves under different power all show single main peak in the absence of long wavelength tails corresponding to a peak wavelength of 2.06 μm, indicating an ideal band to band transition occurring in the absorber. Figure.1(d) plots the band diagram of the whole device. Considering the feasibility of the convergence for the commercial software SILVACO 2022, only two cycles of InGaAs/GaAsSb is plotted on behalf of the whole periods of InGaAs/GaAsSb absorber. As shown in the band diagram, the conduction offset between InGaAs/GaAsSb absorber and AlGaAsSb barrier is large (about 1eV) while the valence band offset almost vanishes. The inserted wide band gap AlGaAsSb barrier facilitate the electron transport to the N side contact and shorten the band bending length in the narrow band gap absorber under operating bias so that the GR current would be suppressed.

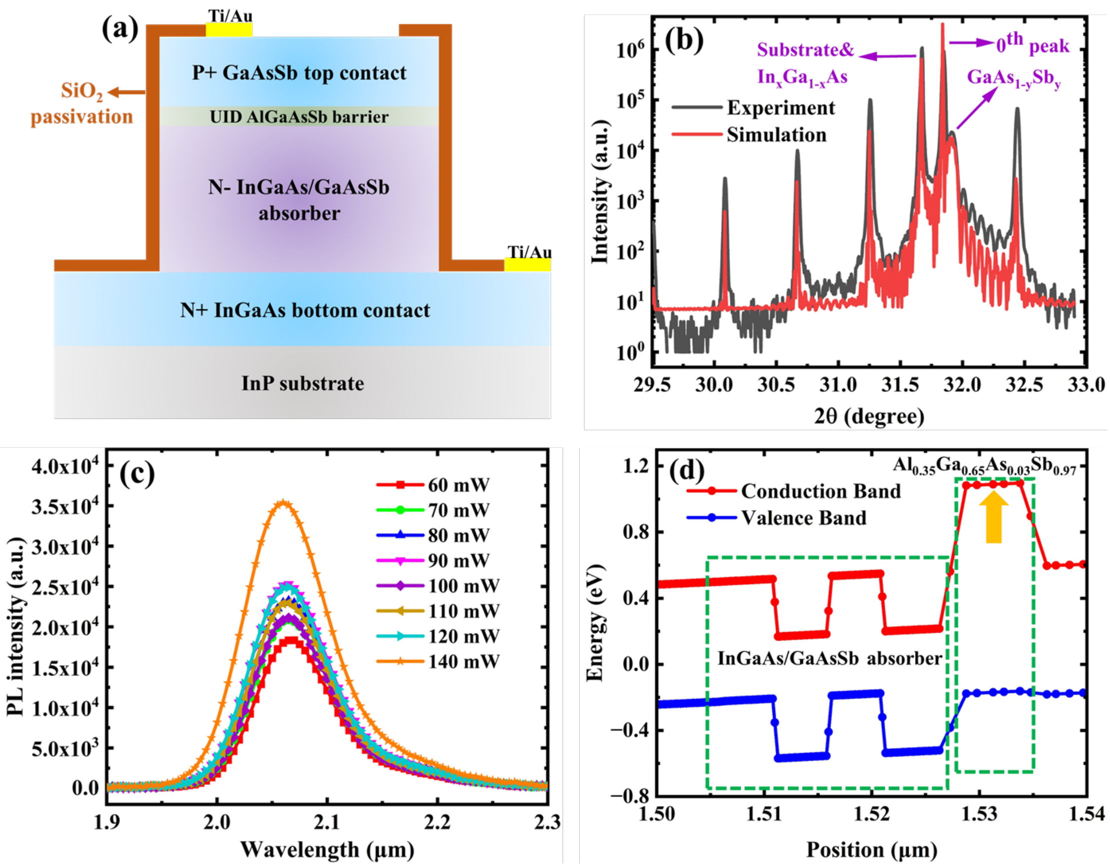


**Fig.1**(a) Schematic configuration of the pBn type InGaAs/GaAsSb photodetector. (b) XRD results of the epilayer grown on InP substrate. (c) Power dependent PL

spectra of the epilayer grown on InP substrate. (d) Simplified band diagram of the InGaAs/GaAsSb photodetector.

The temperature dependent dark current characteristic of the fabricated device with D=100 μm is shown in Figure.2. Under a reverse bias of -1 V, the dark current density is $1.57\times10^{-4}$ A/cm$^2$ at 220 K and rises up to $2.4\times10^{-3}$ A/cm$^2$ at 300 K.

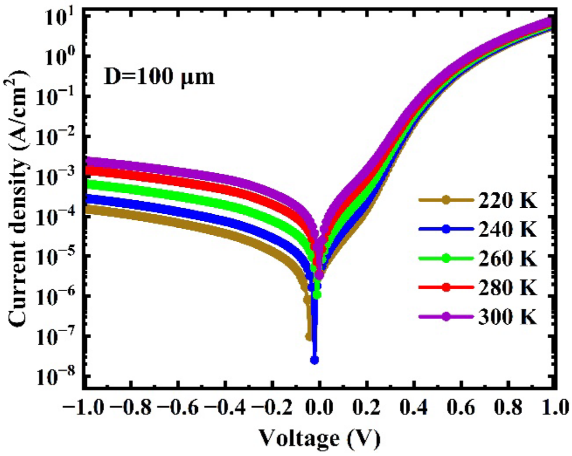


Fig.2. Temperature dependent dark current characteristic of InGaAs/GaAsSb photodetector

The relative spectral responsivity under different bias voltage is shown in Figure.3(a). As the reverse bias increase, the relative spectral responsivity saturated at -1 V. Therfore, we measured absolute responsivity of the device at the temperature range from 220 K to 300 K, as shown in Figure.3(b). The cutoff wavelength is 2.2 μm at 300 K which coincides well with the band diagram simulation result and the PL spectra. Moreover, the peak absolute responsivity rises with the increasing temperature from 0.22 A/W at 220 K to 0.30 A/W at 300 K. The absolute response value at 2 μm reaches 0.06 A/W. The temperature dependent spectral response characteristic could be explained by the temperature dependent characteristic of the quantum efficiency. The minority carrier diffusion length increases when the temperature increase, leading to a positive correlation between the quantum efficiency and the temperature, hence the absolute responsivity [26,27] .

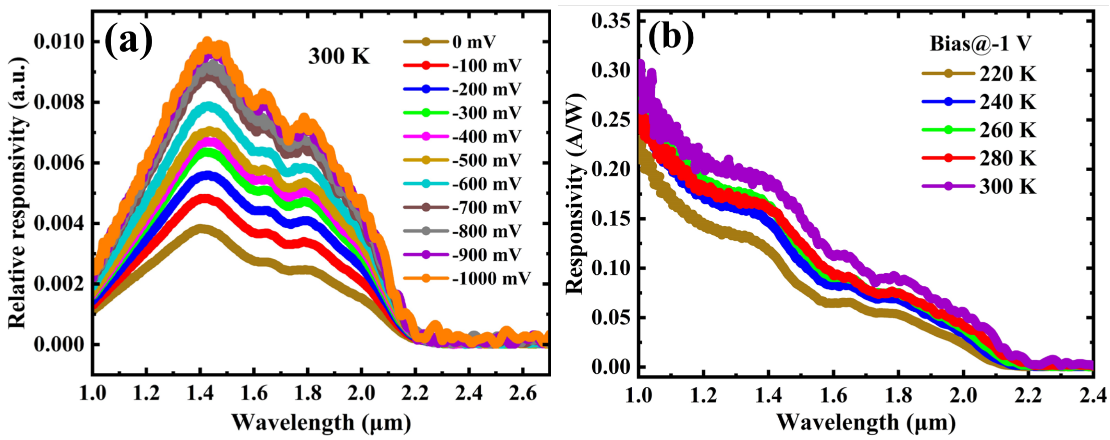


Fig.3(a) Relative spectral response under different reverse bias voltage. (b) Temperature dependent absolute responsivity at temperature from 220 K to 300 K.

Figure 4 shows the calculated detectivity of the pBn InGaAs/GaAsSb photodetector at temperature range from 220 K to 300 K. At 300 K, the detectivity at 2.1 μm is $2.0\times10^9$ $cm\cdot Hz^{1/2}/W$ under the saturated reverse bias of -1 V.

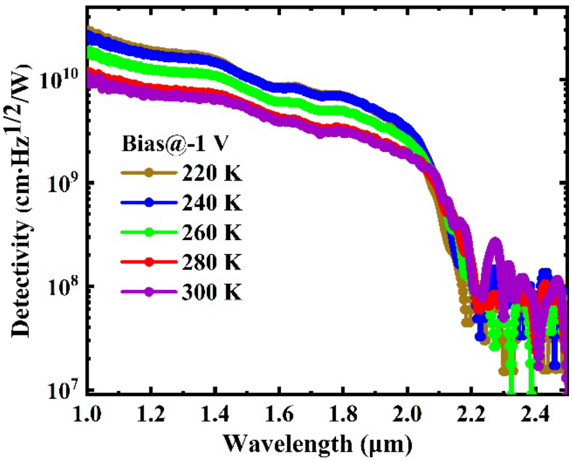


Fig.4 Specific Detectivity of InGaAs/GaAsSb pBn photodetector at temperature range from 220 K to 300 K.

Table.1 summarize the dark current characteristic and the absolute spectral response of the state of-the-art InGaAs/GaAsSb device. Our device presents low dark current but further suppression of the dark current is needed since the unintentional doping of AlGaAsSb barrier layer actually presents a light P type doping profile, which is opposite to the InGaAs/GaAsSb absorber doping polarity leading to remaining of

GR current component（**Maybe we can concern the actual doping profile as a reason for high GR current?**）. Also, the optimization of the wide bandgap optical window between the absorber and the top contact is required to further enhance the carrier collection efficiency of the device to increase the absolute spectral response.

Table.1 Dark current characteristics of reported works on InGaAs/GaAsSb photodetectors

| | Device characteristic | Dark current density ($A/cm^2$) | Responsivity (A/W) or Quantum efficiency（%） |
|---|---|---|---|
| I. Shafir et al[24)] | pBp structure (InP barrier) | $8.3\times10^{-3}$ (-0.1 V, 300 K) | 37 % at 2.2 μm (-0.1 V, 300 K) |
| Jingyi Wang et al[28)] | InAlAs/AlAsSb window | $3.48\times10^{-4}$ (-1 V, 300 K) | N/A |
| Y. Uliel et al[29)] | mesa and planar | mesa: $1.5\times10^{-3}$ (-50 mV, 300 K) planar: $1.2\times10^{-3}$ (-50 mV, 300 K) | mesa:37 % at 2.18 μm (-0.1 V,300 K) planar: lower than mesa type device |
| Zongheng Xie et al[30)] | dual band structure | $3.78\times10^{-2}$ (-1 V, 300 K) for e-SWIR range | 13.5 % at 2 μm |
| This work | pBn structure | $2.4\times10^{-3}$ (-1 V, 300 K) | 0.06 A/W at 2 μm |

In summary, we demonstrate a pBn type SWIR photodetector based on InGaAs/GaAsSb absorber and AlGaAsSb barrier. InGaAs/GaAsSb epi-layer grown on InP substrate with both high structural and optical properties are obtained. Low dark current density down to $1.57\times10^{-4}$ $A/cm^2$ at 220 K and $2.4\times10^{-3}$ $A/cm^2$ at 300 K are achieved, respectively. The room dark current density is lower than most of the reported works. The peak absolute responsivity under saturated operating bias reached 0.30 A/W at 300 K , corresponding to a peak specific detectivity of 2.0× $10^9$ cm·Hz$^{1/2}$/W.


## Acknowledgements

This work is funded by the National Science and Technology Major Project of China (Grant No. 2018YFE0200900).


## References


1) Ruud W. M Hoogeveen, J van der A Ronald, and Albert P. H Goede, Infrared Physics & Technology **42**, 1 (2001).

2) Chulyeon Lee, Hwajeong Kim, and Youngkyoo Kim, npj Flexible Electronics **5**, 10 (2021).

3) Vasanthi Sivaprakasam, Di Lin, and Michael K.Gemar Yetzbacher, Heath E.Portier, Joel M.Watnik, Abbie T., optics express **31**, 5443 (2023).

4) Ritobrata Sur, Kai Sun, Jay B Jeffries, Ronald K Hanson, Randy J Pummill, Travis Waind, David R Wagner, and Kevin J Whitty, Applied Physics B **116**, 33 (2014).

5) Zhang Yong-Gang, Zhang Xiao-Jun, Zhu Xiang-Rong, Li Ai-Zhen, and Liu Sheng, Chinese Physics Letters **24**, 2301 (2007).

6) O. Gravrand, J. Rothman, C. Cervera, N. Baier, and B. Fieque, Journal of Electronic Materials **45**, 4532 (2016).

7) M. Kopytko and A. Rogalski, Sensors and Actuators, A. Physical, 339 (2022).

8) W. E. Tennant, Donald Lee, Majid Zandian, Eric Piquette, and Michael Carmody, Journal of Electronic Materials **37**, 1406 (2008).

9) Antoni Rogalski, Journal of Alloys & Compounds **371**, 53 (2004).

10) A. Rogalski, Infrared Physics & Technology **54**, 136 (2011).

11) Tennant, William, E., Cockrum, C., A., Gilpin, J., B., and Kinch, Journal of Vacuum Science & Technology B Microelectronics & Nanometer Structures (1992).

12) Smiri Badreddine, RS Joshya, Demir Ilkay, Saidi Faouzi, Altuntas Ismail, Delphine

Lagarde, Cedric Rober, Marie Xavier, and Maaref Hassen, Optics & Laser Technology **148**, 107714 (2022).

13) Yage Liu, Yingjie Ma, Xue Li, Yi Gu, Tao Li, Luhong Wan, Xiumei Shao, and Haimei Gong, IEEE Journal of Quantum Electronics **57**, 1 (2021).

14) Yong Gang Zhang, Yi Gu, Xiu Mei Shao, Xue Li, and Jia Xiong Fang, Chinese Physics B **27**, 128102 (2018).

15) L. Zhou, Y. G. Zhang, Y. Gu, X. Y. Chen, Y. Y. Cao, and H. S. B. Y. Li, Journal of Alloys & Compounds **576**, 336 (2013).

16) Xuefei Li, Jianming Xu, Tieshi Wei, Wenxian Yang, Shan Jin, Yuanyuan Wu, and Shulong Lu, Crystals **11**, 1590 (2021).

17) Yingjie Ma, Yonggang Zhang, Xingyou Chen, Yi Gu, Yanhui Shi, Wanyan Ji, and Ben Du, Journal of Physics D: Applied Physics **51**, 145106 (2018).

18) Suho Park, Jiyeon Jeon, Vivek Mohan More, Rochelle Safia Lee, Youryang Seo, Minkyung Kim, Phuc Dinh Nguyen, Minkyeong Kim, Jong Su Kim, and Yeongho Kim, Applied Surface Science **581**, 152421 (2022).

19) SP Xi, Y Gu, YG Zhang, XY Chen, L Zhou, AZ Li, and Hsby Li, Journal of Crystal Growth **425**, 337 (2015).

20) Ben Du, Yi Gu, Xing-You Chen, Ying-Jie Ma, Yan-Hui Shi, Jian Zhang, and Yong-Gang Zhang, Japanese Journal of Applied Physics **57**, 060302 (2018).

21) Yi Gu, Li Zhou, Yonggang Zhang, Xingyou Chen, Yingjie Ma, Suping Xi, and Haosibaiyin Li, Applied Physics Express **8**, 022202 (2015).

22) K Miura, Y Iguchi, M Tsubokura, and Y Kawamura, Journal of applied physics **113** (2013).

23) Justin Easley, Christopher R Martin, Martin H Ettenberg, and Jamie Phillips, Journal of Electronic Materials **48**, 6025 (2019).

24) I Shafir, DC Elias, D Memram, N Sicron, and M Katz, Infrared Physics & Technology **125**, 104217 (2022).

25) Jonathan Petticrew, Yuting Ji, Benjamin White, Axel Evirgen, Jean-Luc Reverchon, Mark Hopkinson, Chee Hing Tan, and Jo Shien Ng, Semiconductor Science and Technology **38**, 025002 (2022).

26) D Cohen-Elias, N Snapi, O Klin, E Weiss, S Shusterman, T Meir, and M Katz, Applied Physics Letters **111** (2017).

27) I Shafir, D Cohen-Elias, N Snapi, O Klin, E Weiss, N Sicron, and M Katz, Infrared Physics & Technology **105**, 103210 (2020).

28) Jingyi Wang, Zhiyang Xie, Liqi Zhu, Xinbo Zou, Xuyi Zhao, Wenfu Yu, Ruotao Liu, Antian Du, Qian Gong, and Baile Chen, IEEE Electron Device Letters **43**, 757 (2022).

29) Y Uliel, D Cohen-Elias, N Sicron, I Grimberg, N Snapi, Y Paltiel, and M Katz, Infrared Physics & Technology **84**, 63 (2017).

30) Zongheng Xie, Zhuo Deng, Xinbo Zou, and Baile Chen, IEEE Photonics Technology Letters **32**, 1003 (2020).